AD-A265 633

IENTATION PAGE

Form Approved
OBM No. 0704 0188

1. Agency Use Only (Leave blank).	2. Report Date. December 1992	3. Report Type and Dates Covered. Final - Journal Article

4. Title and Subtitle.
A Normal-Mode Analysis of Rapid Teleconnections in a Numerical Weather Prediction Model. Part II. Tropical and Extratropical Aspects

5. Funding Numbers.
Contract
Program Element No 0601153N
Project No. RM35G84
Task No.
Accession No. DN659750
Work Unit No. 6.1-OMP

6. Author(s).
Ronald Gelaro

7. Performing Organization Name(s) and Address(es).
Naval Research Laboratory
Atmospheric Directorate
Monterey, CA 93943-5006

8. Performing Organization Report Number.
JA 432:055:90

9. Sponsoring/Monitoring Agency Name(s) and Address(es).
Office of Naval Research
Arlington, VA 22217

10. Sponsoring/Monitoring Agency Report Number.
JA 432:055:90

11. Supplementary Notes.
Published in Monthly Weather Review.

12a. Distribution/Availability Statement.
Approved for public release; distribution is unlimited.

12b. Distribution Code.

13. Abstract *(Maximum 200 words).*

A unique analysis is applied to the normal modes to the U.S. Navy's global operational numerical weather prediction model to investigate time-varying responses in the tropics and extratropics to tropical Pacific sea surface temperature anomalies. With this new analysis, the modes are partitioned according to their latitudinal variances. This allows the response energy to be separated into tropical and extratropical contributions. The partitioned responses are derived by grouping those modes whose fractional variance within a prescribed latitudinal band $\delta\mu$ exceeds some threshold value β. Since the parameters $\delta\mu$ and β may be chose arbitrarily, this technique greatly increases the flexibility of the normal-mode diagnostic approach.

The partitioned responses reveal distinct differences between the evolution and vertical scales of the dominant modes in the tropics and extratropics. In the tropics, the structure is dominated by the external and a medium-depth internal mode. The internal mode is determined by the profile of the large-scale divergence and subsequent rotational wind (Walker circulation) response driven by enhanced convection. In the extratropics, the dominant structure is equivalent barotropic. The external rotational modes grow rapidly within the extratropics in an manner that suggest that meridional propagation alone does not fully explain the growth of the extratropical response.

93 [illegible] 048

14. Subject Terms.
Planetary boundary layer, ocean mixed layer, air-sea interaction

15. Number of Pages.
14

16. Price Code.

17. Security Classification of Report.	18. Security Classification of This Page.	19. Security Classification of Abstract.	20. Limitation of Abstract.
Unclassified	Unclassified	Unclassified	SAR

Reprinted from MONTHLY WEATHER REVIEW, Vol. 120, No. 12, December 1992
American Meteorological Society

A Normal-Mode Analysis of Rapid Teleconnections in a Numerical Weather Prediction Model. Part II: Tropical and Extratropical Aspects

RONALD GELARO

A Normal-Mode Analysis of Rapid Teleconnections in a Numerical Weather Prediction Model. Part II: Tropical and Extratropical Aspects

RONALD GELARO

Naval Research Laboratory, Monterey, California

(Manuscript received 5 June 1991, in final form 2 March 1992)

ABSTRACT

A unique analysis is applied to the normal modes of the U.S. Navy's global operational numerical weather prediction model to investigate time-varying responses in the tropics and extratropics to tropical Pacific sea surface temperature anomalies. With this new analysis, the modes are partitioned according to their latitudinal variances. This allows the response energy to be separated into tropical and extratropical contributions. The partitioned responses are derived by grouping those modes whose fractional variance within a prescribed latitudinal band $\delta\mu$ exceeds some threshold value β. Since the parameters $\delta\mu$ and β may be chosen arbitrarily, this technique greatly increases the flexibility of the normal-mode diagnostic approach.

The partitioned responses reveal distinct differences between the evolution and vertical scales of the dominant modes in the tropics and extratropics. In the tropics, the structure is dominated by the external mode and a medium-depth internal mode. The internal mode is determined by the profile of the large-scale divergence and subsequent rotational wind (Walker circulation) response driven by enhanced convection. In the extratropics, the dominant structure is equivalent barotropic. The external rotational modes grow rapidly within the extratropics in a manner that suggests that meridional propagation alone does not fully explain the growth of the extratropical response.

1. Introduction

This is Part II of a study investigating global-scale interactions between the tropics and extratropics using the normal modes of a global numerical weather prediction (NWP) model. The main objectives of this study are to demonstrate the rapid response of the global circulation to tropical forcing anomalies and to investigate the evolution and dynamic structure of this response in a sophisticated NWP model. The model used is part of the Navy Operational Global Atmospheric Prediction System (NOGAPS) described by Hogan and Rosmond (1991).

The analysis in Part I (Gelaro 1992, hereafter referred to as GI) was conducted from a global perspective, in which the normal modes, in conjunction with standard difference field diagnostics, were used to analyze the model response to sea surface temperature (SST) anomalies in the tropical Pacific. It was shown that the response was dominated by external and medium-depth internal rotational modes that grew rapidly, obtaining a significant fraction of their steady-state amplitudes during the first two weeks of the simulations. A wavenumber decomposition of the extratropical wave pattern supported these results, revealing the rapid growth of the pattern between days 7 and 10 of the simulations. The results demonstrated that the modes could be used effectively to identify and monitor the growth of the dominant vertical and horizontal structures of the global response, and in some cases, to make conclusions about the physical processes involved. These conclusions, however, were limited by the global nature of the calculations presented in GI.

In this paper, the normal-mode analysis is extended to investigate *separately* the tropical and extratropical components of the responses. This spatial segregation of the response provides further insights into the response mechanisms. In sections 2 and 3, a new technique is developed whereby the model normal modes are partitioned according to their latitudinal variances in order to define the tropical and extratropical contributions to the response energy. The development of this technique follows directly from the normal-mode formulation of a simple expression for the total energy in the linearized model, as described in the Appendix. In section 4, this partitioning technique is used to analyze the results of the model experiments conducted in GI. The reader is referred to sections 2 and 3 of that paper for a description of those experiments and an overview of the model response. In section 5, selected response fields are projected onto the modes to corroborate the analysis and to provide physical interpretations of the results. Finally, conclusions and suggestions for future research are discussed in section 6.

Corresponding author address: Dr. Ronald Gelaro, Naval Research Laboratory, Atmospheric Directorate, Monterey, CA 93943-5006.

2. Latitudinal variance

As shown in the Appendix, the energy of a single normal mode J may be written in the form

$$E_J = \gamma \alpha_J \alpha_J^* \Lambda_J, \tag{1}$$

where

$$\Lambda_J = \sum_n \sum_{n'} \underbrace{\left[(\hat{\Phi}_n^J \hat{\Phi}_{n'}^{J*} + \hat{\zeta}_n^J \hat{\zeta}_{n'}^{J*} + \hat{D}_n^J \hat{D}_{n'}^{J*}) \right.}_{\text{A}} \times \underbrace{\left. \int_{\mu_1}^{\mu_2} P_n^m P_{n'}^m d\mu \right]}_{\text{B}} \tag{2}$$

and the limits of integration are written generally for the purposes of the following discussion. As shown schematically in (2), Λ_J depends on two factors. Factor A describes the fractional contributions of the various forms of energy to the total energy of mode J, while factor B describes the latitudinal variance of the mode. As discussed in the Appendix, the structures of the modes have been normalized such that $\Lambda_J = 1$ when E_J is equal to the global total energy of mode J. In that case, (1) reduces to Eq. (1) in GI.

If we consider some component of the total energy of mode J, $E_J' \leq E_J$, then Λ_J can have any value $0 \leq \Lambda_J \leq 1$, which may be interpreted as a weight equal to the ratio E_J'/E_J. Since it is independent of the data, Λ_J thus provides a convenient way to examine the energetics of the modes in further detail. For example, from factor A in (2) we see that the fractional contribution of available potential energy to the total energy of mode J is given by

$$\Lambda_J^{(\mathrm{PE})} = \sum_n \hat{\Phi}_n^J \hat{\Phi}_n^{J*}. \tag{3}$$

In the present study, factor B in (2) is of primary interest as it can be evaluated within some latitudinal range $\delta\mu$ to obtain the fraction of the total variance of mode J within that range. This information, in turn, can be used to define a measure of the response energy in that range. Strictly speaking, for arbitrary values of $\delta\mu$ there may be nonzero contributions from those terms in B for which $n \neq n'$. It can be shown, however, that these terms do not contribute significantly to the variances and are thus neglected in the present context. A consequence of this simplification is that the integrand in B becomes a positive-definite function that has equal value in the same latitudinal bands in each hemisphere. Therefore, care should be taken when selecting $\delta\mu$ since; for example, no distinction can be made between the variance of mode J in the ranges 5°–10°N and 5°–10°S.

We seek a way of using B in (2) to determine whether mode J contributes to the tropical or extratropical response in the experiments described in GI. For the T47 model truncation used in this study, the functional values of P_n^m are defined on a Gaussian transform grid that has 72 latitudinal points. For our purposes, we define the tropics as extending eight Gaussian latitudes from the equator in both hemispheres. This corresponds to the latitudinal belt between approximately 19°N and 19°S. The remaining area in both hemispheres is defined as the extratropics. Accordingly, we define for each mode the discrete variance estimates

$$\Lambda_J^{(\mathrm{trop})} \equiv \sum_n \sum_{i=29}^{44} [P_n^m(\mu_i)]^2 w_i \tag{4}$$

and

$$\Lambda_J^{(\mathrm{xtrop})} \equiv \sum_n \sum_{i=1,i=45}^{28,72} [P_n^m(\mu_i)]^2 w_i \tag{5}$$

for the tropics and extratropics, respectively, where w_i is the weight given to the functional value of P_n^m at Gaussian latitude μ_i (Abramowitz and Stegun 1965), with μ_1 the southernmost latitude and μ_{72} the northernmost latitude. The summation over i in (4) thus encompasses an equatorially symmetric latitudinal band with poleward boundaries at μ_{29} and μ_{44} in the Southern and Northern hemispheres, respectively. The summation over i in (5) encompasses two separate latitudinal bands bounded by μ_1 and μ_{28} in the Southern Hemisphere, and by μ_{45} and μ_{72} in the Northern Hemisphere. Note that, with these definitions, the tropical and extratropical variance factors for mode J are related to one another by $\Lambda_J^{(\mathrm{trop})} = 1 - \Lambda_J^{(\mathrm{xtrop})}$.

3. Partitioning the modes

The values of $\Lambda_J^{(\mathrm{trop})}$ and $\Lambda_J^{(\mathrm{xtrop})}$ can be used effectively as a means of classifying mode J as tropical or extratropical. In this way, an estimate of the tropical energy, for example, can be obtained by computing the quantity

$$E^{(\mathrm{trop})} = \sum_{J \in \mathcal{T}} E_J, \tag{6}$$

where E_J is the total energy of mode J as given by (A6), but the sum in (6) includes only those modes for which $\Lambda_J^{(\mathrm{trop})}$ exceeds some threshold value β for tropical modes. This set of tropical modes is denoted by $\mathcal{T}$ and defined formally as

$$\mathcal{T} \equiv \{J | \Lambda_J^{(\mathrm{trop})} \geq \beta\}. \tag{7}$$

By defining the tropical energy as in (6), we have used the values of $\Lambda_J^{(\mathrm{trop})}$ as selection criteria for tropical modes rather than as weighting functions in a summation over all modes as might be inferred; for example, from (1). In this way, a sharper, but still realistic, separation is obtained between the characteristics of the tropical and extratropical contributions to the global energy. Also, this approach is somewhat easier

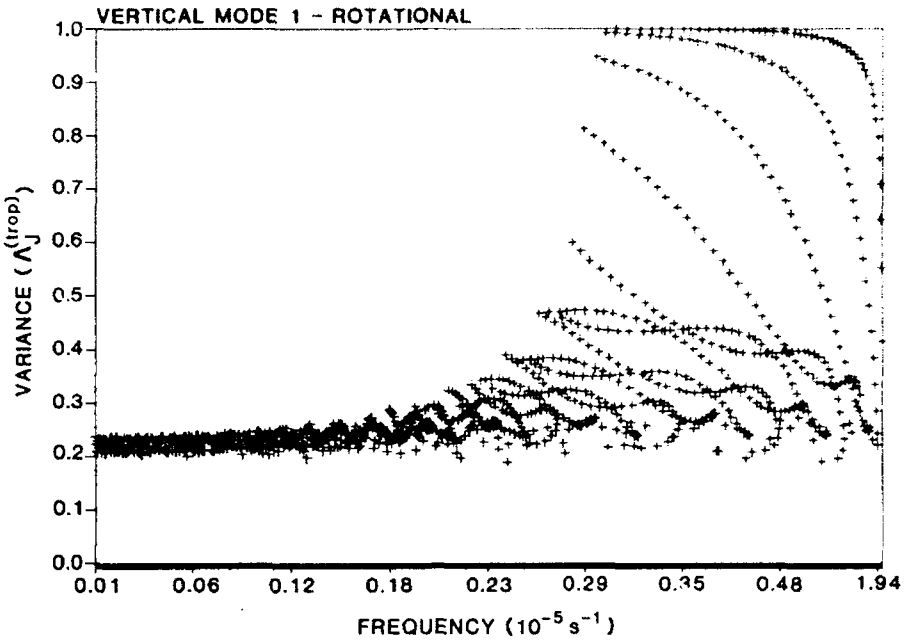

FIG. 1. Values of the variance factors $\Lambda_J^{(trop)}$ for the external rotational modes plotted as a function of their natural periods. The values along the ordinate correspond to the fraction of the modal variance between 19°N and 19°S.

to interpret physically since each term in (6) accounts for the total variance of mode J.

Clearly, the key to partitioning the modes as in (7) is to define a reasonable threshold value β for identifying tropical (or extratropical) modes. Unfortunately, there is no a priori way of knowing what threshold values of $\Lambda_J^{(trop)}$ and $\Lambda_J^{(xtrop)}$ adequately separate the two groups of modes. The most straightforward approach is simply to plot the variance factors as a function of the natural frequencies ω_J of the modes in order to see where a natural separation might exist.

Figures 1 and 2 show the values of $\Lambda_J^{(trop)}$ corresponding to the rotational and eastward gravitational modes, respectively, for the external ($l = 1$) vertical mode. Again, these values are computed for $\delta\mu$ extending from approximately 19°N to 19°S, as given

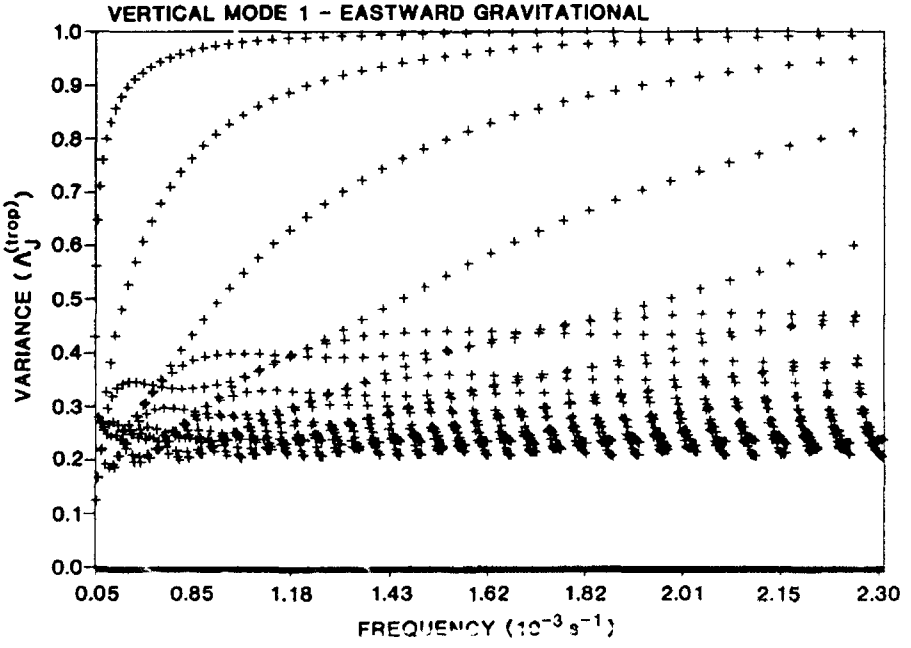

FIG. 2. As in Fig. 1 except for the external eastward gravitational modes.

by (4), and describe the fraction of the total variance of mode J that occurs within this latitudinal band. The frequencies are ordered from smallest to largest according to their absolute values. This ordering is from largest to smallest spatial scales for the gravitational modes, and from smallest to largest spatial scales for the rotational modes. As in GL, we consider all modes except the zonally symmetric ones corresponding to $m = 0$. In both figures, there appears to be a lower cutoff near $\Lambda_J^{(\mathrm{trop})} = 0.2$, indicating that very few modes have less than 20% of their variance in the tropics. In other words, there are no purely extratropical modes [i.e., values at, or near, $\Lambda_J^{(\mathrm{trop})} = 0$] according to this definition. In contrast, note that in both figures there are modes for which $\Lambda_J^{(\mathrm{trop})}$ is very close to one, indicating that nearly all of their variance occurs within the tropics. The value of the lower cutoff depends, in part, on the choice of $\delta\mu$ and increases or decreases, accordingly. In both figures, the values of $\Lambda_J^{(\mathrm{trop})}$ appear to be organized into discrete bands that are downward from left to right for the rotational modes in Fig. 1, and downward from right to left for the eastward gravitational modes in Fig. 2. Each band represents a family of modes having the same meridional scale denoted by the index j, while each mode in that band, or j family, corresponds to a different zonal wavenumber m. There are 47 such families (excluding the zonally symmetric modes) corresponding to the T47 model truncation, in which the number of modes varies from 47 for $j = 1$, down to 1 for $j = 47$.

For the rotational modes in Fig. 1, the $j = 1$ family is the upper-rightmost band and represents the mixed Rossby–gravity modes. Many of these modes are tropically trapped as indicated by their relatively large values of $\Lambda_J^{(\mathrm{trop})}$. The $j = 1$ family for the eastward gravitational modes is the upper-leftmost band in Fig. 2 and corresponds to low-frequency Kelvin modes. As expected, these modes also tend to be trapped and have values close to $\Lambda_J^{(\mathrm{trop})} = 1$. Note that in both figures those modes with large meridional structure (small values of j) have more of their variance in the tropics than those with smaller meridional structure (large values of j). Clearly, there is much more information that can be gleaned from plots of Λ_J for various ranges of $\delta\mu$. For example, it is interesting to note that the rotational modes in Fig. 1 exhibit very little tropical variance for $\omega_J < 2.3 \times 10^{-6}\ \mathrm{s}^{-1}$ (periods greater than 31 days). At this time, it is unclear whether there is some theoretical basis for this sharp cutoff.

Plots such as those in Figs. 1 and 2 for the remaining vertical modes reveal similar patterns for their corresponding frequency ranges. As an example, we show in Fig. 3 values of $\Lambda_J^{(\mathrm{trop})}$ corresponding to the eastward gravitational modes for $l = 5$. For all vertical modes, it was generally found that the modes demonstrated a marked increase in tropical variance for $j \leq 6$. Roughly speaking, most of the modes in these families have values of $\Lambda_J^{(\mathrm{trop})} \geq 0.4$. Based on these figures, we adopted the cutoff value $\Lambda_J^{(\mathrm{trop})} \geq 0.4$ for "tropical" modes, and $\Lambda_J^{(\mathrm{trop})} \leq 0.3$ for "extratropical" modes. Those modes for which $0.3 < \Lambda_J^{(\mathrm{trop})} < 0.4$ are difficult to classify as belonging in one group or the other, and are thus excluded from the analysis. Note that it is only necessary to consider $\Lambda_J^{(\mathrm{trop})}$ in order to identify both the tropical and extratropical modes since $\Lambda_J^{(\mathrm{trop})}$ and $\Lambda_J^{(\mathrm{xtrop})}$ sum to one, as discussed earlier; that is, $\Lambda_J^{(\mathrm{trop})} \leq 0.3$ is synonymous with $\Lambda_J^{(\mathrm{xtrop})} > 0.7$.

It is important to note that, for the threshold values

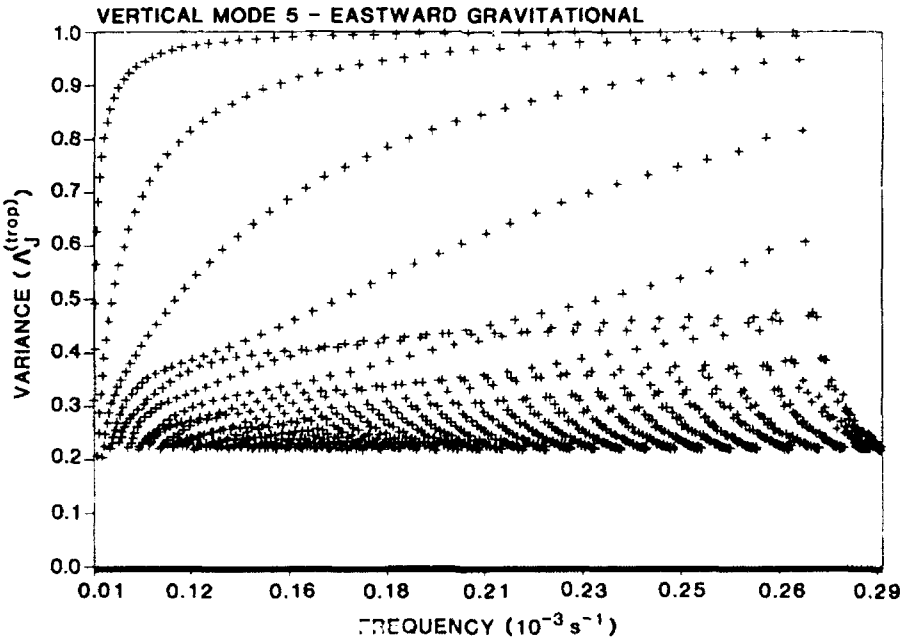

FIG. 3. As in Fig. 1 except for the $l = 5$ eastward gravitational modes.

TABLE 1. The numbers of rotational (RT), eastward gravitational (EG), and westward gravitational (WG) modes classified as "tropical" or "extratropical" for each vertical mode l based on the threshold values $\Lambda_j^{(trop)} \geq 0.4$ and $\Lambda_j^{(xtrop)} \geq 0.7$, respectively.

	Tropical			Extratropical		
l	RT	EG	WG	RT	EG	WG
1	204	204	204	748	748	748
2	203	203	204	746	748	748
3	205	204	204	744	748	744
4	208	205	204	739	747	741
5	215	210	211	733	740	732
6	216	212	217	726	733	722
7	217	215	214	719	729	713
8	224	217	216	709	716	701
9	231	225	227	688	698	675
10	238	234	234	671	679	650
11	241	237	238	657	666	631
12	245	240	246	646	655	670
13	246	245	249	634	651	612
14	254	248	253	630	643	609
15	258	250	259	630	637	604
16	256	254	263	630	634	598
17	255	256	265	632	634	596
18	250	255	271	633	634	593

selected above, the number of horizontal modes of each type is fairly evenly distributed within each group. Table 1 shows the numbers of rotational and eastward and westward gravitational modes in the tropical and extratropical groups for each vertical mode. Roughly speaking, we see that for $l \leq 8$ there are between 200 and 220 tropical modes of each type, and between 710 and 740 extratropical modes of each type for each vertical mode. This ensures that a fair comparison can be made between the relative contributions of each vertical mode to the tropical or extratropical response energy. There are, of course, more extratropical modes than tropical modes because of the difference in the latitudinal ranges $\delta\mu$ used to define each region. For each vertical mode, the two groups account for roughly 85% of the total number of modes in the complete (global) set. That is, 15% of the complete set have values $0.3 < \Lambda_j^{(trop)} < 0.4$, and are not included in either group. Further justification for the threshold values of $\Lambda_j^{(trop)}$ and $\Lambda_j^{(xtrop)}$ selected above are given in the following sections.

4. Tropical and extratropical responses

In this section, the normal-mode partitioning technique developed in sections 2 and 3 is used to analyze the tropical and extratropical contributions to the global response energy in the western Pacific SST anomaly experiment described in GI. Figure 4 shows the response energy in each region for all mode types as a function of vertical mode l for the two 5-day mean periods corresponding to days 1–5 and days 21–25 of the simulations. Analogous to the global energy calculations shown in GI, we plot for each vertical mode a normalized response energy that, for the tropical energy in Fig. 4a, takes the form

$$E_l^{(trop)} = \frac{1}{E^{(trop)}} \sum_{j \in T_l} E_j, \tag{8}$$

where the summation includes only tropical modes that have equivalent depth h_l (denoted by the set T_l) and, for notational convenience, the superscript δ used in GI to denote a response field is implied. For the extratropical energy, we plot for each vertical mode the quantity $E_l^{(xtrop)}$, which we define by analogy to (8) by summing over only the set of extratropical modes $\mathcal{M}_l$ and normalizing by the extratropical energy $E^{(xtrop)}$.

The profiles in both regions are qualitatively similar during days 1–5, with relative maximums at $l = 4$ and $l = 16$. For the extratropical modes in Fig. 4b, the external modes are also relatively energetic during this time. By days 21–25, the external modes dominate the profiles in both regions, but the relative contributions

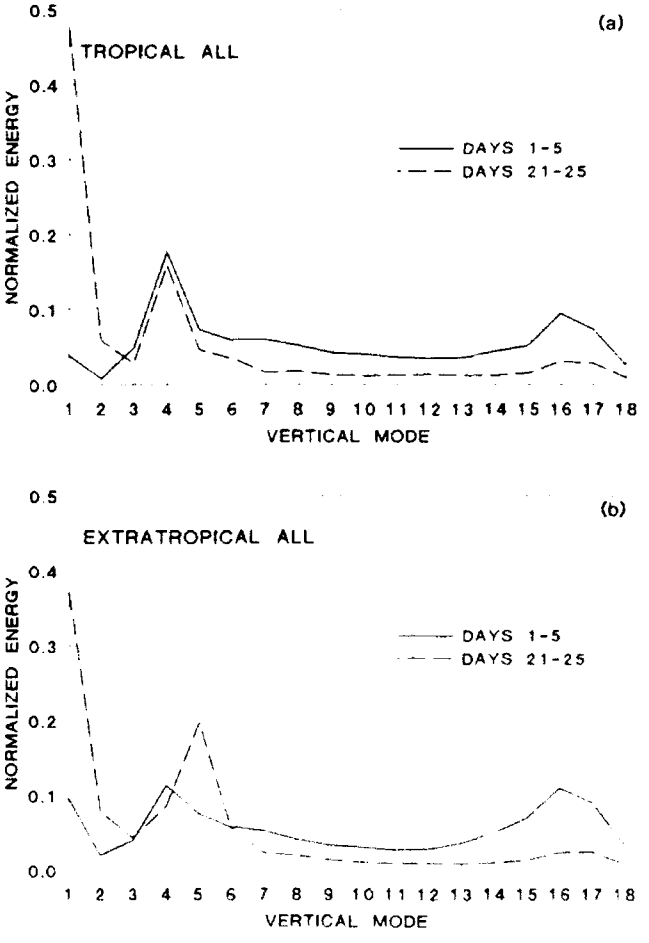

FIG. 4. The normalized response energies (a) $E_l^{(trop)}$ and (b) $E_l^{(xtrop)}$ as a function of vertical mode l for all mode types corresponding to days 1–5 (solid) and days 21–25 (dashed) of the experiment described in GI.

from the medium-depth internal modes now differ markedly. In the tropics, $l = 4$ remains the dominant internal mode, while $l = 5$ now dominates in the extratropics. In both regions, only modes corresponding to $l < 6$ contribute significantly by this time.

The evolution of the rotational-mode energy in the tropics and extratropics for vertical modes 1–5 is shown in Fig. 5. Again, the external modes dominate in both regions, but the importance of $l = 4$ in the tropics and $l = 5$ in the extratropics is clearly evident. Interestingly, the rotational modes appear to grow more rapidly in the extratropics. This result, combined with the results in Fig. 12 in GI, which showed that certain modes grow at preferred locations in the midlatitudes, suggests that meridionally propagating tropical wave energy does not completely explain the extratropical response. Also, note the relatively smooth evolution of the dominant extratropical modes compared with those in the tropics. Figure 6 shows that the gravitational modes play a more important role in the overall energy balance in the tropics but, in the long term, are still roughly an order of magnitude smaller than the rotational modes.

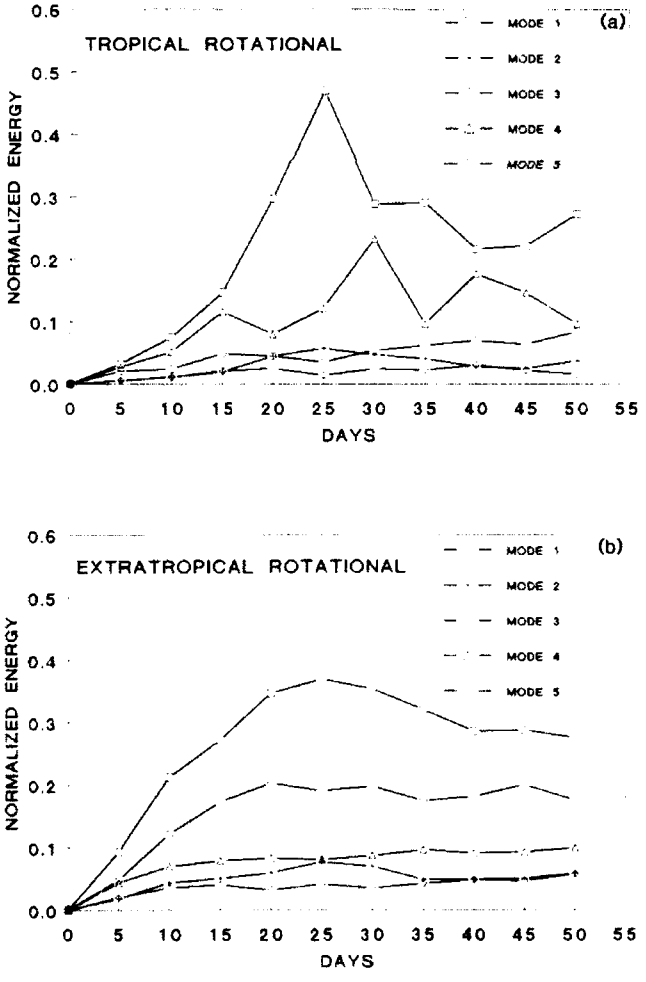

FIG. 5. The evolution of (a) $E_l^{(\mathrm{trop})}$ and (b) $E_l^{(\mathrm{xtrop})}$ for the $l = 1$–5 rotational modes in the GI experiment. The plotted values correspond to 5-day means ending on the days shown along the abscissa.

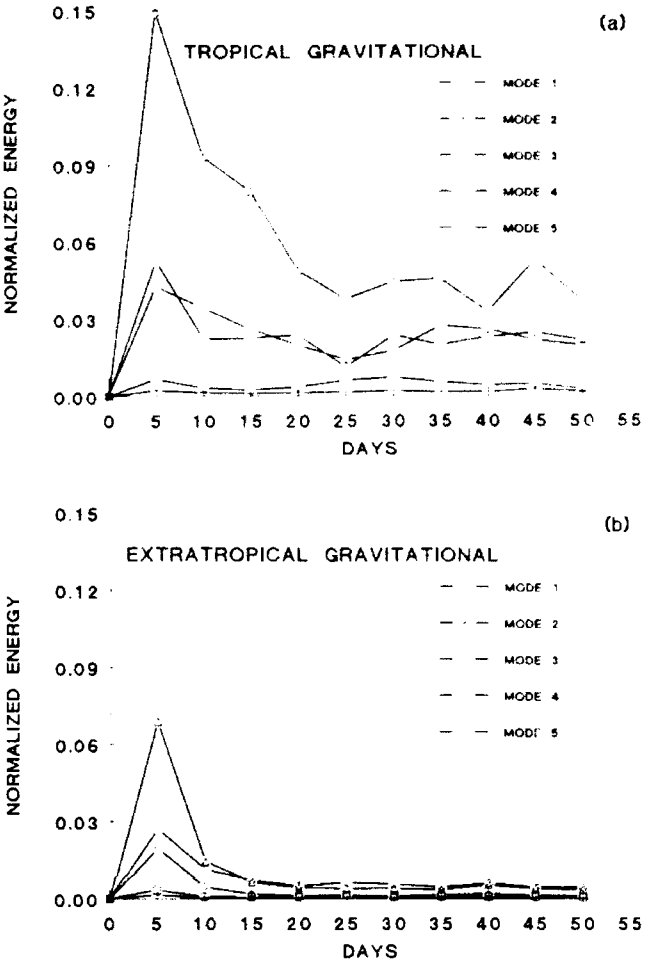

FIG. 6. As in Fig. 5 except for the gravitational modes. Note the different ordinate scale and smaller energies than in Fig. 5.

Since, strictly speaking, the results in Figs. 4–6 reveal only information about the structure of the responses, an interesting question is whether the predominant response modes in the tropics and extratropics are actually of different dynamical origins. The predominance of the external modes in Fig. 5b is consistent with the equivalent barotropic structure of the extratropical response (cf. Fig. 8 in GI). In a strongly sheared environment, this response has its maximum amplitude near tropopause level (e.g., Held 1983). As discussed in GI, however, and shown here in Fig. 7, the linearization used in the present study yields an external mode that is nearly barotropic throughout the troposphere and thus is inadequate for describing this structure completely. Thus, the simultaneous evolution of $l = 5$ in the extratropics, which has its maximum amplitude at approximately 250 mb (Fig. 7), undoubtedly is also a manifestation of the growth of the equivalent barotropic response. This conclusion is confirmed in section 6.

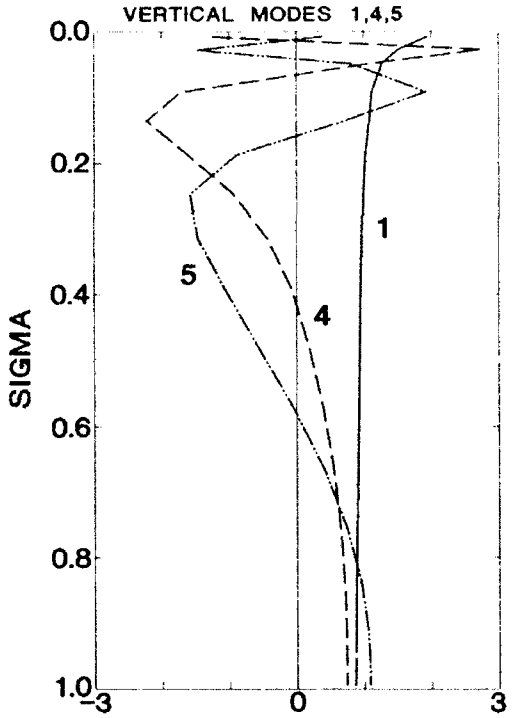

FIG. 7. Vertical modes 1, 4, and 5 of the NOGAPS model, based on the parameter values shown in Table 1 of GI (signs are arbitrary).

In contrast with the extratropics, there is no obvious barotropic phenomenon in the tropics that explains the strong external-mode response in Fig. 5a. A growth mechanism for these modes, however, has been demonstrated by Lim and Chang (1986) (hereafter referred to as LC), whereby vertical shear acts to produce an external response from purely internal (e.g., convective) forcing. LC argue that internal forcing initially produces an internal-mode response with upper-level divergence and lower-level convergence that, by stretching the lower atmospheric column and compressing the upper one, leads to an internal-mode rotational response through conservation of potential vorticity. Over a period of several days, vertical wind shear acts to couple the internal and external rotational modes, resulting in a transfer of energy to the latter. With this in mind, it is interesting to note that the $l = 4$ rotational response in Fig. 5a is preceded by a strong $l = 4$ gravitational (i.e., divergent) response, as shown in Fig. 6a. The projection of the gravitational response onto $l = 4$ is explained by Fig. 8a, which shows a vertical profile of the 30-day mean divergence response averaged over the region of anomalous SST in the GI experiments. The structure of the profile, characterized by a sharp peak with maximum divergence just below 100 mb, and a deep, but weaker, layer of convergence below 200 mb that extends to the surface, is very similar to that of vertical mode 4 (see Fig. 7; signs are arbitrary). As suggested by LC, a rotational response develops with similar vertical structure, as indicated by the growth of $l = 4$ in Fig. 5a and supported by Fig. 8b, showing the vertical profile of the 30-day mean rotational zonal-wind response averaged between 11°N–11°S and 90°–170°W. The profile in Fig. 8b reveals the enhanced Walker circulation in the central and eastern Pacific with strong westerlies at upper levels and weaker easterlies below. A response with similar vertical structure, but opposite sign, occurs to the west of the SST anomaly in the Indian Ocean (not shown).

Finally, note that in contrast with the $l = 5$ response in Fig. 5b the $l = 4$ response in Fig. 5a grows slowly and then fluctuates significantly about some quasi-steady state. The time scale of these fluctuations is comparable with that observed in time series of the model's convective rainfall (Hogan 1991, personal communication). The external modes in Fig. 5a also grow slowly at first, but then grow much more rapidly after the second week of the simulation when the growth at $l = 4$ has leveled off. Despite the delayed rapid growth of the external modes, it is puzzling that there is no observable lag in their initial growth compared with $l = 4$. This detail may be lost either as a result of the partitioning procedure [specifically, the choices for the latitudinal ranges $\delta\mu$ used to define (4) and (5), or the threshold value β in (7)] or the temporal resolution of these results. Another possibility is that the theory proposed by LC is somewhat oversimplified, having been derived from a much simpler model. Nonetheless, the growth rate and magnitude of the external response agree well with those obtained by LC and the contrasting character of the growth curves in Figs. 5a and 5b seems to indicate that the predominant responses in each region are of different dynamical origins.

5. Vertical-mode projections

As indicated above, the results in Figs. 4–6 depend on the variance factors (4) and (5), and in particular, on the threshold value β in (7) used to define the subsets of tropical and extratropical modes. In this section, the upper-tropospheric streamfunction response is projected onto the model normal modes. These projections are done to check the physical plausibility of the partitioned responses discussed in section 5. The projections shown here are totally independent of the partitioning technique used to obtain those results. The contribution to the response from each vertical mode is computed as the difference between the total response field and a response field for which the normal-mode amplitudes corresponding to that vertical mode have been set to zero; that is, a type of linear initialization is performed. It was decided to use this difference method rather than compute the desired projections directly because of the potential difficulty in reconstructing the fields from only a single vertical mode. Projections of the streamfunction response at 150 and 300 mb are presented since they are close to the levels

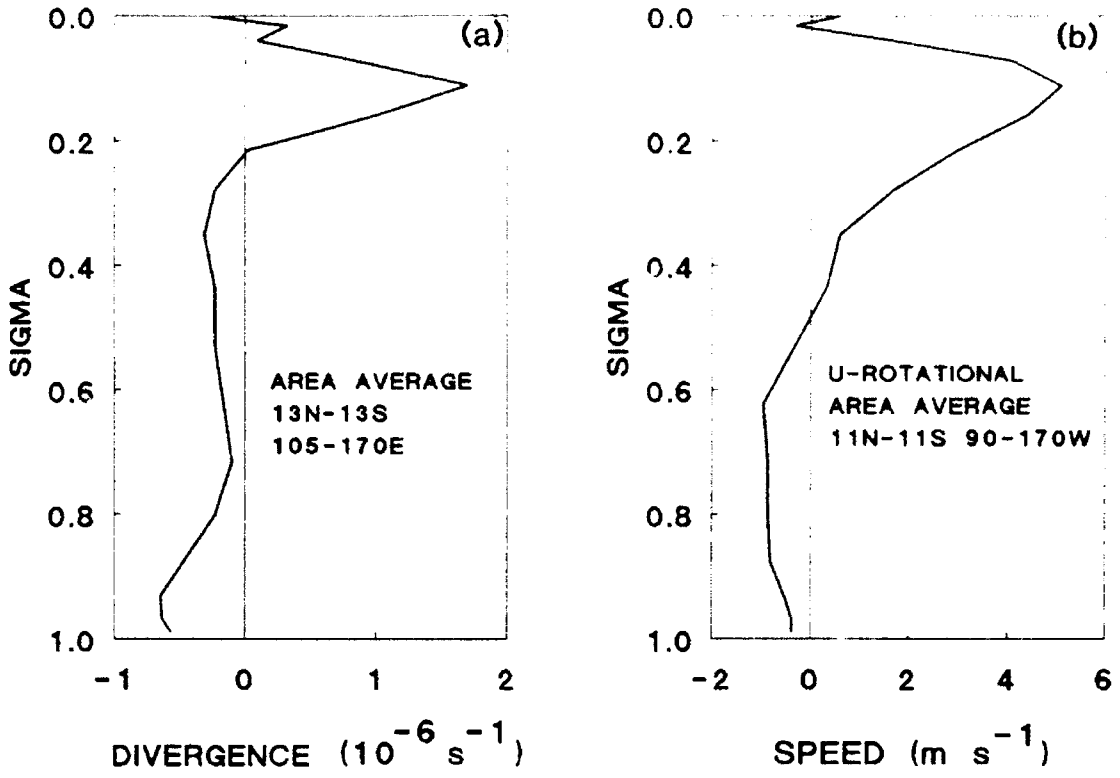

FIG. 8. Area-averaged 30-day mean response profiles of (a) divergence in the region of increased SST and (b) rotational zonal-wind speed over the central and eastern tropical Pacific in the GI experiment. The profile in (b) may be thought of as representing the Pacific Walker circulation. Note the similarity of both profiles to the structure of vertical mode 4 shown in Fig. 7.

of maximum amplitude for vertical modes 4 and 5, respectively (see Fig. 7).

Figure 9 shows the 30-day mean streamfunction response at 300 mb. The total response is shown in Fig. 9a, while the projections onto vertical modes 1, 4, and 5 are shown in Figs. 9b, 9c, and 9d, respectively. As expected, the total response in Fig. 9a shows a strong extratropical stationary wave pattern in both hemispheres and some indication of anomalous equatorial westerlies in the central Pacific. The extratropical wave pattern, particularly in the Northern Hemisphere, projects strongly onto vertical mode 1 (Fig. 9b) as well as vertical mode 5 (Fig. 9d), in agreement with the results in Fig. 5b for the extratropical response energy. Furthermore, the results in Fig. 9 confirm that the growth of $l = 1$ and $l = 5$ in Fig. 5b is, in fact, a manifestation of the equivalent barotropic structure of this response. For example, note that most of the variance in the circulation anomalies over North America in Fig. 9a is accounted for by the projections in Figs. 9b and 9d. In the tropics, there is a weak, but clearly identifiable, projection of the equatorial Pacific westerlies in Fig. 9b, while the projection in Fig. 9d has very little amplitude anywhere in the tropics. This is consistent with the relatively weak contribution from $l = 5$ in Fig. 5a. As expected, the projection onto $l = 4$ in Fig. 9c has considerably less amplitude anywhere at 300 mb in accordance with the vertical structure of this mode as shown in Fig. 7.

Figure 10 is the same as Fig. 9, except for a 30-day mean streamfunction response at 150 mb. Again, the total response in Fig. 10a shows a strong stationary wave pattern in both hemispheres, but also has considerably more amplitude in the tropics than the streamfunction response at 300 mb. This is consistent with the strong response at $l = 4$ (which has its maximum amplitude near this level) in Fig. 5a and with the fact that the tropical response has its maximum amplitude near tropopause level. In Fig. 10a, anomalous westerlies to the east of the forcing region are clearly defined by the strong cross-equatorial streamfunction gradient that extends across most of the Pacific, while there are strong anticyclones to the northwest and southwest of the forcing. The latter features are well-known responses to an equatorially symmetric heat source (e.g., Blackmon et al. 1983; Palmer and Mansfield 1986; Sardeshmukh and Hoskins 1988). The extratropical wave pattern projects strongly onto vertical mode 1 in Fig. 10b, while the tropical response features have only weak projection onto this mode. Note the similarity between the character and amplitude of the projections in Figs. 9b and 10b, reflecting

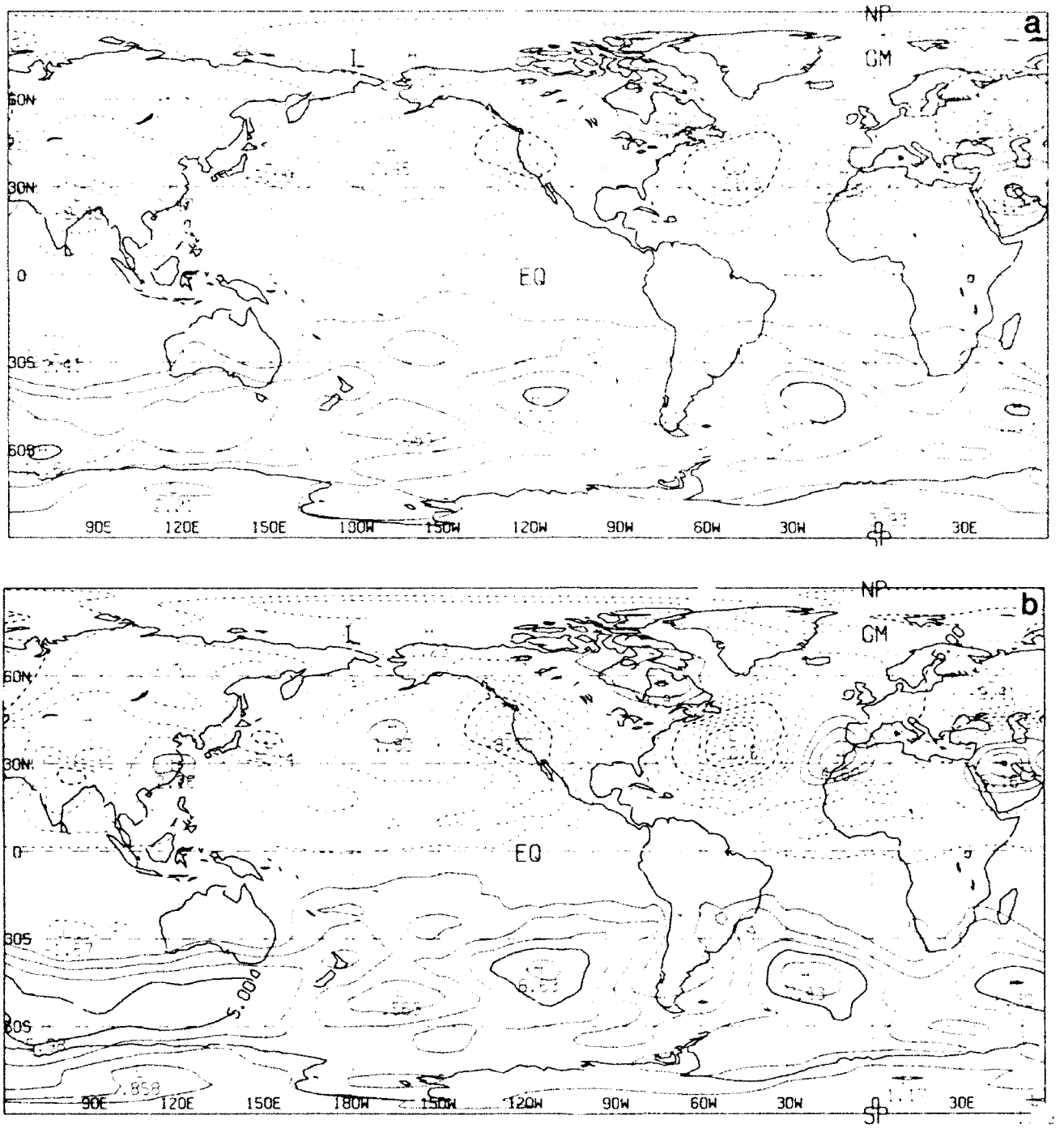

FIG. 9. The 30-day mean 300-mb streamfunction response in the GI experiment for (a) the total response and for the projections of the response onto (b) vertical mode 1, (c) vertical mode 4, and (d) vertical mode 5. The contour interval is 2.5×10^6 m^2 s^{-1}, with negative values denoted by dashed lines.

the nearly barotropic structure of the external modes. In contrast, Fig. 10c shows that the tropical response projects strongly onto vertical mode 4, while the middle- and high-latitude response has much less amplitude for this vertical mode. Note, for example, the near absence of the North American response in Fig. 10c. Again, these results clearly support the results in Fig. 5a showing the strong contribution from $l = 4$ to the tropical response energy. Conversely, the relative lack of amplitude in the extratropics in Fig. 10c is in agreement with the relatively weak contribution from $l = 4$ to the extratropical response energy in Fig. 5b. As ex-

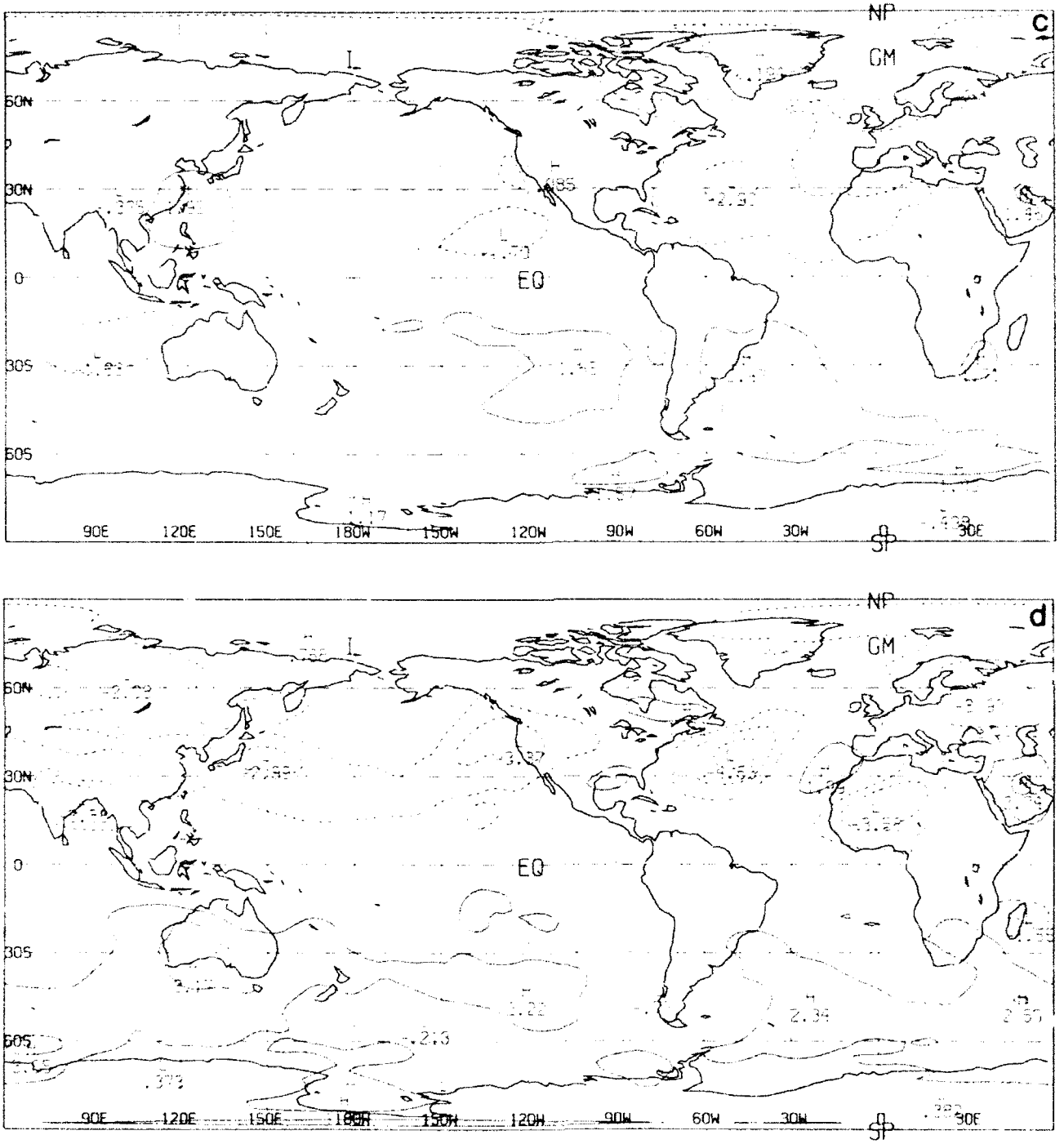

FIG. 9. (*Continued*)

pected, the projection onto vertical mode 5 in Fig. 10d is negligible at 150 mb. In summary, the results in Figs. 9 and 10 support the partitioned responses in Fig. 5.

6. Summary and conclusions

Global-scale interactions between the tropics and extratropics were examined in terms of the normal modes of a sophisticated NWP model. A new technique was developed whereby the modes were partitioned according to their latitudinal variances in order to define the tropical and extratropical components of the model total energy. The development of this technique followed from a straightforward derivation of the model total energy in normal-mode form, in which the latitudinal structures of the modes appeared as explicit

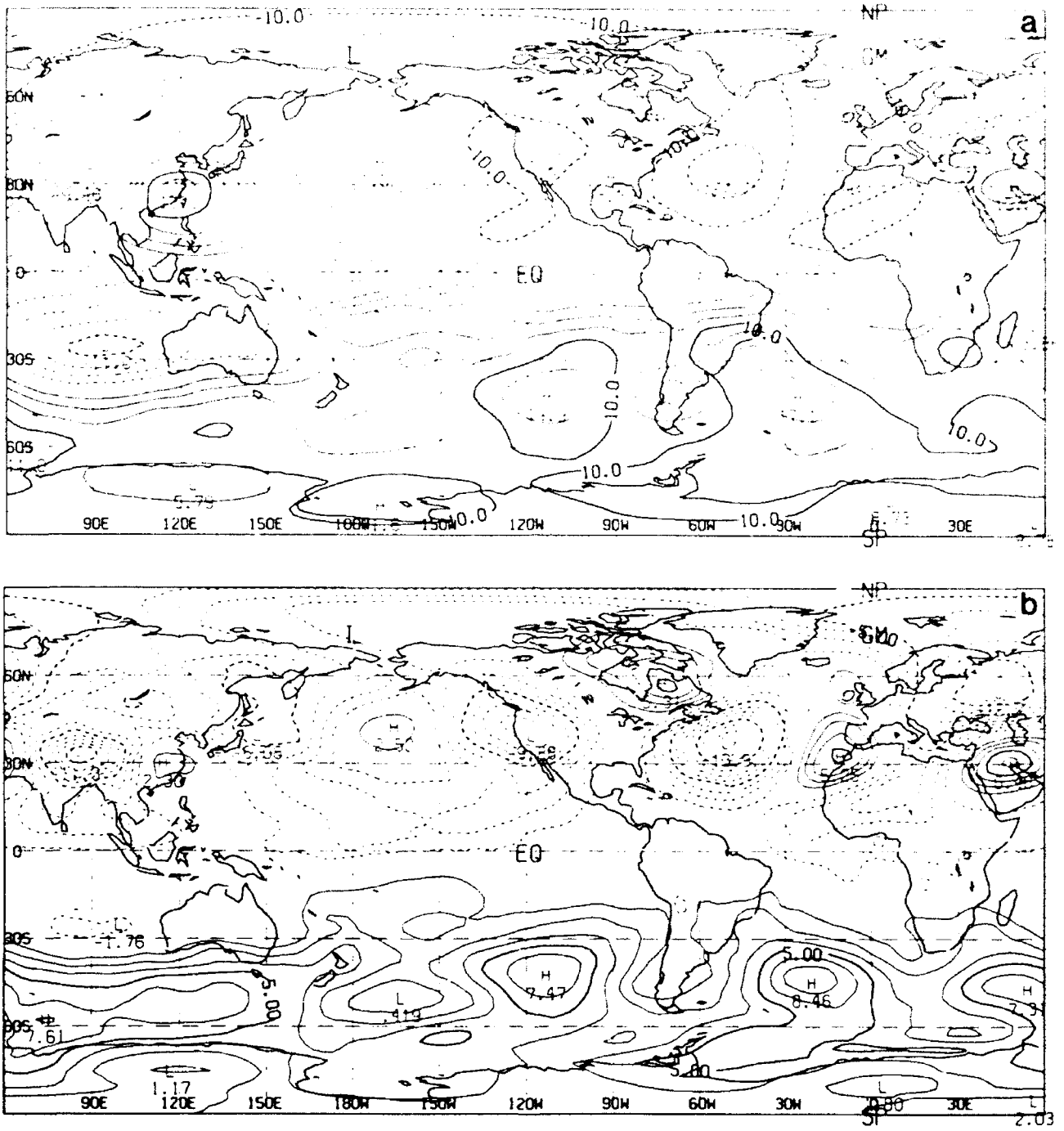

FIG. 10. As in Fig. 9 except at 150 mb.

terms in an integral equation. The partitioned responses were derived from those modes whose fractional variance within either region exceeded a predefined threshold value. We applied this partitioning technique to analyze the results of a series of experiments conducted by Gelaro (1992), who used the U.S. Navy's operational global forecast model to demonstrate the rapid atmospheric response to SST anomalies in the tropical Pacific. The analysis revealed the different structural characteristics of the tropical and extratropical responses obtained in those experiments, and provided insight into the mechanisms that govern their evolution. Furthermore, it showed that the normal modes are a powerful and flexible tool for diagnosing the behavior of complicated models.

Both external and internal rotational modes were

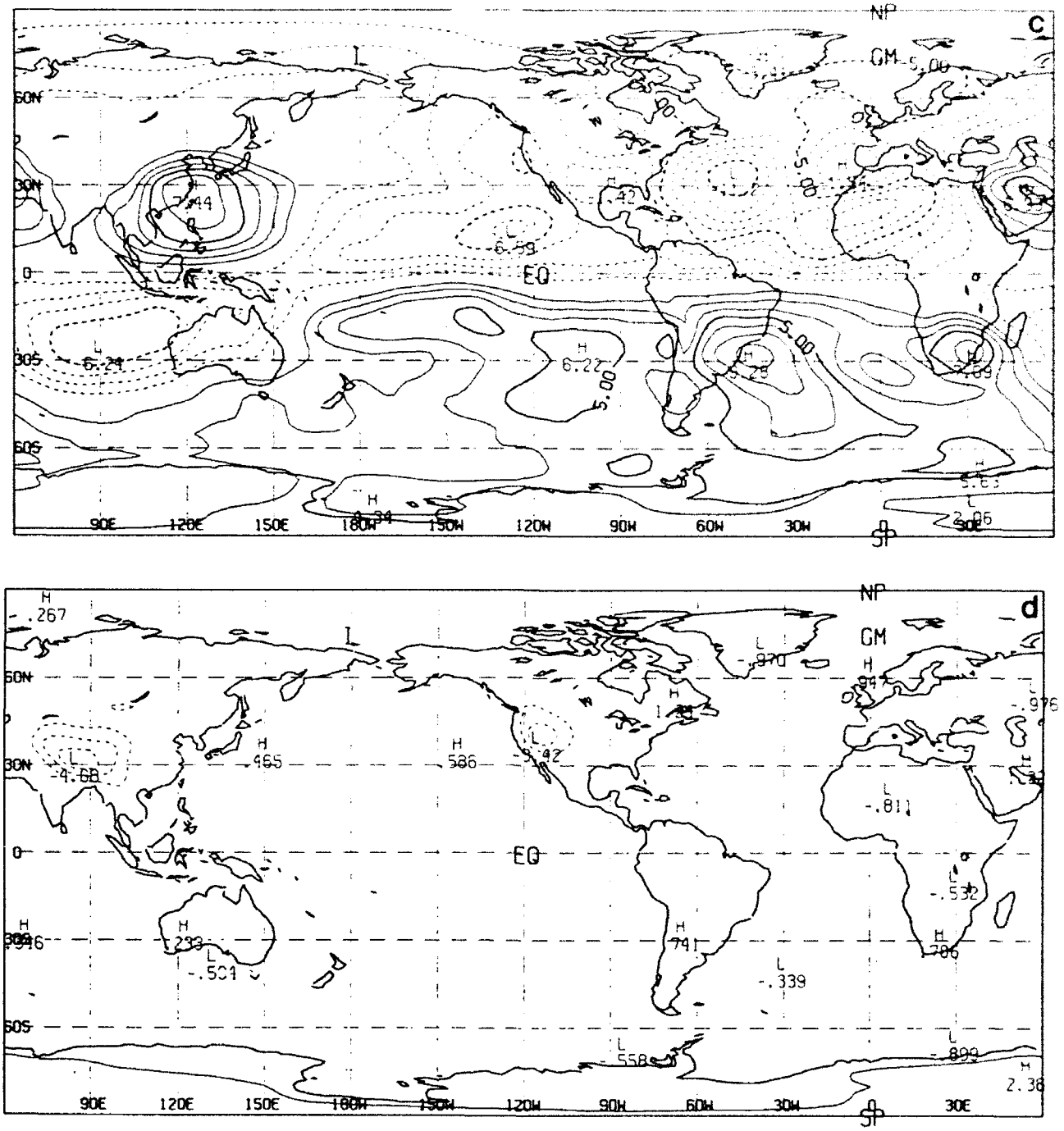

FIG. 10. (*Continued*)

shown to contribute significantly to the tropical and extratropical responses. Of particular interest was that the dominant internal-mode responses projected onto different vertical modes in each region, with vertical mode 4 dominating in the tropics and vertical mode 5 dominating in the extratropics. This distinction, in addition to the different temporal behavior of the tropical and extratropical modes, was indicative of the different dynamical origins of the dominant modes in each region.

In the extratropics, the internal and external modes evolved simultaneously throughout the simulations, with the latter clearly dominating the response. Vertical-mode projections of the upper-tropospheric streamfunction response confirmed that both modes were required to resolve the strongly equivalent baro-

tropic structure of the extratropical response, which obtained its maximum amplitude near tropopause level. As in the global analysis presented in Gelaro (1992), the response evolved rapidly, with much of its long-term character well developed after the first week. The projection of this response onto vertical mode 5 (which has its maximum amplitude near 250 mb, but changes sign in the middle troposphere) does not itself appear to be of any dynamical significance. Rather, this seems to be an indication that the no-motion basic state used to derive the modes is a poor approximation of the model's very energetic and strongly sheared midlatitude basic state. This in no way invalidates the applicability of normal modes derived from simple basic states, as demonstrated by their successful use in nonlinear normal-mode initialization schemes (e.g., Andersen 1977; Hogan et al. 1991), as well as in model diagnostic studies (e.g., Errico et al. 1988). It does imply, however, that care must be taken when interpreting the physical mechanisms that produce a particular modal response.

In contrast, the simple basic state used in these calculations is a considerably better (though not optimal) approximation of the model's tropical basic state. Accordingly, the predominance of vertical mode 4 in the tropics was shown to be dynamically significant, being entirely consistent with the structure of the large-scale divergence and zonal-wind fields there. The strong responses at this vertical scale in both the gravitational and rotational modes appeared to agree with the results of Lim and Chang (1986), who showed that convective heating can produce a hierarchy of internal-mode responses culminating in a transfer of energy to the external rotational modes. However, it was not possible to verify this completely from the results presented here. Nonetheless, the relatively slower and more variable evolution of the rotational response in the tropics was in clear contrast with the smooth and surprisingly rapid evolution of the extratropical response.

It is important to bear in mind that the results of this analysis (as well as the success of the partitioning method itself) depend on the latitudinal ranges $\delta\mu$ used to define the variance factors $\Lambda_j^{(\text{trop})}$ and $\Lambda_j^{(\text{extrop})}$, and on the threshold values β used to define the tropical and extratropical modes. Although the values chosen for these parameters yielded physically reasonable results (as verified, for example, by the streamfunction projections in section 6), additional work is required to investigate the robustness of these results and their sensitivity to the aforementioned parameters. In particular, by choosing geographically separated latitudinal ranges to define the tropics and extratropics (rather than having a common latitudinal boundary at 19° in each hemisphere), or by using more stringent threshold values for grouping the modes, we might minimize the risk of "smearing" the responses in each region. Other improvements, including additional simulations and greater sampling resolution than the 5-day means presented here, might also resolve some of these issues. Despite these limitations, the results clearly demonstrate the usefulness of the normal modes as diagnostic tools that, because of the inclusion of normal-mode initialization schemes in most global forecast models, can be readily developed.

Acknowledgments. The author wishes to thank the reviewers for their helpful comments and suggestions for improving the manuscript. Special thanks are extended to Dr. T. Murphree of the Naval Postgraduate School for his valuable discussion and comments on this work, and to Mr. S. Bishop for his help in preparing the figures.

Funding for this effort was provided by the Office of Naval Technology through the Predictive Systems Development Program (Program Element 62435N). Contribution 432:056:90.

APPENDIX

Normal-Mode Energetics in NOGAPS

In a continuous linear system, the total kinetic plus available potential energy E per unit mass can be written

$$E = \frac{1}{8\pi}\int_0^1\int_0^{2\pi}\int_{-1}^{1}[\Phi\epsilon^{-1}\Phi - \psi\nabla^2\psi \quad \chi\nabla^2\chi] \times d\mu d\lambda d\sigma, \quad (A1)$$

where ψ is the streamfunction, χ is the velocity potential, Φ is the geopotential, and ϵ is a differential operator of the vertical coordinate σ (Errico 1987). The variables λ and μ are the longitude and sine of the latitude, respectively, and ∇^2 is the horizontal Laplacian operator in spherical coordinates.

For our purposes, we seek the normal-mode transform of (A1). Because the NOGAPS model is spectral in both horizontal dimensions and uses vorticity ζ and divergence D as the dependent variables for the velocity field (Hogan and Rosmond 1991), an appropriate form of (A1) for this study is

$$E = \frac{1}{4}\int_0^1\int_{-1}^{1}\sum_m\sum_n\sum_{n'}[c^2\Phi_n^m\epsilon^{-1}\Phi_{n'}^{m*} + b^2r_n r_{n'}(\zeta_n^m\zeta_{n'}^{m*} + D_n^m D_{n'}^{m*})]P_n^m P_{n'}^m d\mu d\sigma, \quad (A2)$$

in which ζ_n^m, D_n^m, and Φ_n^m are spherical harmonic coefficients; P_n^m is an associated Legendre polynomial of degree m and order n; $r_n = a^2/n(n+1)$ derives from the spectral form of the Laplacian operator, where a is the radius of the earth; and an asterisk denotes a complex conjugate. The factors $b = \sqrt{2}\Omega$ and $c = \sqrt{2\Omega^2a^2}$ are dimensional constants in which Ω is the angular velocity of the earth. In obtaining (A2) we have utilized the orthogonal relationship between

Fourier functions with unlike indices and the condition that; for example, $\zeta_n^{-m} = \zeta_n^{m*}$ for real ζ.

To obtain the normal-mode representation of (A2), we expand the dependent variables in the form

$$(\zeta_n^m, D_n^m, \Phi_n^m)^{\mathrm{T}} = \sum_l \sum_j \alpha_J \mathbf{S}_n^l \hat{\mathbf{H}}_n^J z_l, \qquad (A3)$$

where the superscript T denotes a transpose, α_J is the amplitude of mode J, $\hat{\mathbf{H}}_n^J = (\hat{\zeta}_n^J, \hat{D}_n^J, \hat{\Phi}_n^J)^{\mathrm{T}}$ are horizontal structure functions, z_l is a vertical structure function, and $\mathbf{S}_n^l$ is the matrix

$$\mathbf{S}_n^l = \begin{cases} -\Omega a[n(n+1)/gh_l]^{1/2} & 0 & 0 \\ 0 & 0 & 0 \\ 0 & i\Omega a[n(n+1)/gh_l]^{1/2} & 0 \\ 0 & 0 & 1 \end{cases}, \qquad (A4)$$

which ensures that the modes are obtained from a real, symmetric system (Hogan et al. 1991), where g is gravity and h_l is the equivalent depth. The subscript J denotes the index set (l, m, j) so that each normal mode is uniquely identified by its vertical mode l, zonal wavenumber m, and meridional index j. The summation over l in (A3) includes all vertical modes, while the summation over j includes all meridional components with zonal wavenumber m.

If we consider the energy of a single mode J, then (A2), (A3), and (A4) may be combined in the form

$$E_J = \gamma \alpha_J \alpha_J^* \sum_n \sum_{n'} \left[(\hat{\Phi}_n^J \hat{\Phi}_{n'}^{J*} + \hat{\zeta}_n^J \hat{\zeta}_{n'}^{J*} + \hat{D}_n^J \hat{D}_{n'}^{J*}) \times \int_{-1}^{1} P_n^m P_{n'}^m \, d\mu \right], \qquad (A5)$$

where $\gamma = \Omega^4 a^4 / 2gh_l$ gives E_J dimensions of energy per unit mass. The structures of the modes have been normalized such that the summation on the right side of (A5) is unity when E_J is equal to the *global total energy* of mode J. In that case, there are nonzero contributions from only those terms for which $n = n'$ and (A5) reduces to the simple form

$$E_J = \gamma \alpha_J \alpha_J^*. \qquad (A6)$$

REFERENCES

Abramowitz, M., and I. A. Stegun, 1965: *Handbook of Mathematical Functions*. Dover, 1046 pp.

Andersen, J. H., 1977: A routine for normal mode initialization with non-linear correction for a multi-level spectral model with triangular truncation. ECMWF Internal Report 15, 42 pp. [Available from the European centre for Medium-Range Weather Forecasts, Shinfield Park, Reading RG2 9AX, England.]

Blackmon, M. L., J. E. Geisler, and E. J. Pitcher, 1983: A general circulation study of January climate anomaly patterns associated with interannual variation of equatorial Pacific sea surface temperatures. *J. Atmos. Sci.*, **40**, 1410–1425.

Errico, R. M., 1987: A Description of software for determination of normal modes of the NCAR community climate model. NCAR Tech. Note, TN-277+STR, 86 pp. [NTIS PB89-113989.]

——, E. H. Barker, and R. Gelaro, 1988: A determination of balanced normal modes for two models. *Mon. Wea. Rev.*, **116**, 2717–2724.

Gelaro, R., 1992: A normal-mode analysis of rapid teleconnections in a numerical weather prediction model. Part I: Global aspects. *Mon. Wea. Rev.*, **120**, 2897–2913.

Held, I. M., 1983: Stationary and quasi-stationary eddies in the extratropical troposphere: Theory. *Large-Scale Dynamical Processes in the Atmosphere*, B. Hoskins and R. Pearce, Eds., Academic Press, 127–168.

Hogan, T. F., and T. Rosmond, 1991: The description of the Navy Operational Global Atmospheric Prediction System's spectral forecast model. *Mon. Wea. Rev.*, **119**, 1786–1815.

——, ——, and R. Gelaro, 1991: The NOGAPS forecast model: A technical description. NOARL Report 13, 212 pp. [NTIS AD-A247 216.]

Lim, H., and C.-P. Chang, 1986: Generation of internal- and external-mode motions from internal heating: Effects of vertical shear and damping. *J. Atmos. Sci.*, **43**, 948–957.

Palmer, T. N., and D. A. Mansfield, 1986: A study of wintertime circulation anomalies during past El Niño events using a high resolution general circulation model. II: Variability of the seasonal mean response. *Quart. J. Roy. Meteor. Soc.*, **112**, 639–660.

Sardeshmukh, P. D., and B. J. Hoskins, 1988: The generation of global rotational flow by steady idealized tropical divergence. *J. Atmos. Sci.*, **45**, 1228–1251.